Extreme value statistics of mid-latitude atmospheric variability with present-day and increased CO_2 concentration.

Alessandro dell'Aquila[1], Mara Felici[2,3], Valerio Lucarini[2,4] Paolo M. Ruti[1],

Antonio Speranza[2], Renato Vitolo[2] *

July 6, 2007

[1] *ENEA, via Anguillarese 301 – 00060 S. Maria di Galeria, Roma, SP 091 Italy*

[2] *PASEF – Physics and Applied Statistics of Earth Fluids, Dipartimento di Matematica ed Informatica, Università di Camerino, Via Madonna delle Carceri – 62032 Camerino (MC), Italy*

[3] *Dipartimento di Matematica U. Dini, Università di Firenze,*

Corresponding author address: Dr. Renato Vitolo, PASEF, Department of Mathematics and Informatics, University of Camerino, via Madonna delle Carceri, 62032 Camerino (MC), Italy. E-mail: renato.vitolo@unicam.it

viale Morgagni 67/A – 50134 Firenze, Italy

[4] *Dipartimento di Fisica, Università di Bologna,*

viale Berti Pichat 6/2 – 40126 Bologna, Italy

Abstract

The General Circulation Model ECHAM4.6 is run under perpetual January conditions with two different values of CO_2: the present concentration and five times as much. For each case, time series of two indexes of mid-latitude wave activity are computed. The mean activity of baroclinic waves and of planetary waves decreases slightly, following the decrease of the mean baroclinicity of the system. Inference of extreme values is performed by estimating the parameters of the Generalised Extreme Value (GEV) distribution from sequences of maxima over data blocks of fixed length extracted from the time series. The sensitivity and goodness-of-fit of the inferences are assessed by various graphical and numerical tools. The results reveal no marked differences in the statistics of extreme values between the cases with 1 and 5 CO_2 and also suggest that the often invoked approach of relating changes of the extremes to changes in the mean and standard deviation of the bulk statistics is not reliable. Maps corresponding to the dates of the extremes (block maxima) of the indexes show that the relative weight of the wave activity of the Atlantic sector increases with CO_2 concentration.

PACS: 02.50.Tt, 02.70.-c, 47.11.-j, 92.60.Bh, 92.70.Gt

1. Introduction

Recently, we have investigated different aspects of the general circulation of the atmosphere within the framework of either very simplified models or state-of-the-art GCMs, namely:

1. the statistical properties, specifically extreme value statistics, of a baroclinic model of intermediate complexity for the atmospheric mid-latitudes (Lucarini et al. 2006c,d; Felici et al. 2006a,b);

2. the description of wave propagation in the mid-latitude atmosphere of state-of-the-art coupled GCMs (simulations for the IPCC report) and associated products such as re-analyses (Lucarini et al. 2006a; Ruti et al. 2006; Dell'Aquila et al. 2005).

While in the papers of item 1 the procedures concerning extreme statistics and its inference are well settled, in the papers quoted in item 2, dynamically oriented climate metrics aimed at capturing the basic statistical properties of the fundamental features of the mid-latitude atmospheric variability - *e.g.* synoptic baroclinic waves and planetary waves - have been introduced with the purpose of auditing GCMs and reanalyses. In this paper our purpose is to join the two research streams described above, performing statistical analysis of extreme values of dy-

namically oriented metrics. The basic meteo-climatic problem we focus on is: what is the sensitivity of the extreme statistics of mid-latitudinal disturbances to CO_2 increase? The issue is a rather complex and controversial one and it is not easy to deduce, from existing literature, a clear cut scientific formulation.

The northern hemisphere mid-latitude variability is mainly driven by large-scale processes, which affect, at different spatial and temporal scales, the variability of surface parameters (*i.e.* precipitation, wind, temperature). The latter parameters are those typically observed in the meteorological networks and stored in the records. Nevertheless, sufficiently long time-series, suitable for statistical analysis of extreme values, are not always available. This has sometimes led the researchers to adopt weaker criteria for the selection of events to be used for inference of statistical extreme models, with all the ensuing problems of reliability. See the discussion in the introduction of Felici et al. (2006a). On a different front statistical analysis of extreme events has been applied to time-series of surface parameters produced by climate models (Zwiers and Kharin 1998; Kharin and Zwiers 2000). With respect to observations, the usage of synthetically generated data has the advantage that it is easier to satisfy the well-known requirements of length and quality of the record, again see Felici et al. (2006a). However, the characterisation on theoretical grounds of a well-defined relation between the sta-

tistical properties of surface fields and those of the driving large-scale processes remains an open (and very hard) problem.

Among the dominant physical processes featured in the mid-latitude atmospheric dynamics, the synoptic waves and the interaction between ultra-long waves and topography are main ingredients. The synoptic traveling waves can be represented as high-frequency high-wavenumber eastward propagating spectral features, characterised by periods of order 2-7 days and by spatial scales of a few thousand Km. These waves can be associated with the release of available energy driven by conventional baroclinic conversion (Blackmon 1976; Speranza 1983; Wallace et al. 1988), so that they are often referred to as baroclinic waves. On the other hand, planetary waves, which interact with orography (Charney and DeVore 1979; Charney and Straus 1980; Buzzi et al. 1984; Benzi et al. 1986) and are catalysed by the sub-tropical jet (Benzi and Speranza 1989; Ruti et al. 2006), play a dominant role in the low frequency-low wavenumber spectral region of stationary waves, whose characteristic time and space scales belong to the interval 10-45 days and 7000-15000 Km respectively (Hansen and Sutera 1986).

The methodological approach of the present work is to analyse the impact of an increase in the atmospheric CO_2 on the extreme value statistics of indexes of wave activity for the large scale atmospheric dynamics. We run a state-of-

the-art GCM in perpetual winter conditions for both present-day and perturbed atmospheric CO_2 concentrations. Therefore, we generate time series of the Wave Activity Index (WAI) and of the Baroclinic Activity Index (BAI), which may be considered as proxies of the intensity of the planetary and synoptic waves, respectively (Benzi et al. 1986; Dell'Aquila et al. 2006; Hansen and Sutera 1986). Extreme value analysis is then performed by fitting Generalised Extreme Value (GEV) distributions (Coles 2001; Felici et al. 2006a,b) on sequences of block-maxima and of block-minima extracted from the generated time series.

An outline of the paper follows. A short description of the model, metrics and statistical inference can be found in Sec. 2. The bulk statistical properties of the two runs are analysed in Sec. 3. The extreme value analysis of the selected metrics is reported in Sec. 4, while the mapping of the extremes onto the sphere is presented in Sec. 5. Conclusions and lines of future research are summarised in Sec. 6.

2. Data and methods

2a. *Description of the model and experimental setup*

The atmospheric model used in this study is ECHAM4.6, an evolution of the model used by Roeckner and Arpe (1995), belonging to the fourth-generation of GCM developed at the Max Planck Institute for Meteorology in Hamburg. It is an evolution of the spectral weather prediction model of the European Centre for Medium Range Weather Forecasts (Simmons et al 1989). ECHAM4 uses the spectral transform method for *dry dynamics* while water vapour, cloud water and trace constituents are advected by using a shape-preserving semi-Lagrangian scheme (Williamson and Rasch 1994). The model atmosphere is resolved in the vertical by 19 layers, from the surface up to 10hPa. The model contains a set of parameterisations for unresolved or not explicitly represented dynamical and physical processes, including radiation (Fouquart and Bonnel 1980; Morcrette 1991), cumulus convection (Tiedke 1989; Nordeng 1994) stratiform clouds (Roeckner 1995), gravity wave drag (Miller et al. 1989), vertical diffusion and surface fluxes, land surface processes and horizontal diffusion. A summary of the design and performance of ECHAM4 can be found in Roeckner and Arpe (1995).

Two simulations have been performed at T30 spectral horizontal resolution,

corresponding approximately to a grid of 3.75×3.75 degrees. The GCM has been run for 600 model winters (30 days each), under perpetual January conditions, with two values of CO_2 concentration: the present concentration (360 ppmv) and five times as much (1800 ppmv). The two runs only differ in the CO_2 concentration: the Sea Surface Temperature (SST) and sea ice cover are kept constant in time and fixed to the January monthly mean. This implies that when evaluating changes in any statistical property of the atmospheric circulation, we are actually estimating a *partial sensitivity* with respect to CO_2 concentration changes, where the ocean properties are *frozen*: the full sensitivity could be obtained only with a full coupled atmosphere-ocean model. We emphasise that the lack of a seasonal cycle in the simulation, due to the fact that the model is run in perpetual winter conditions, is a further simplification, but it allows to avoid the rather delicate problem of filtering out the seasonal modulation from the signal. Moreover, the bulk of the mid-latitude atmospheric processes which might be affected by the climate change, specifically the baroclinic activities, take place under winter conditions.

2b. *Wave Indexes used for the computation of time series*

The 500hPa geopotential height is one of the most relevant variables descriptive of the large scale atmospheric circulation (Blackmon 1976). Therefore, it constitutes a fundamental benchmark for the comparison of different atmospheric datasets of climatological relevance. Our study focuses on the northern hemisphere mid-latitude atmospheric winter variability as described by the 500hPa geopotential height provided by the $1CO_2$ control run and the $5CO_2$ run. Therefore, we consider the latitudinal belt 30°N-60°N, where both the baroclinic and the low frequency planetary wave activity are present in the ECHAM4.6 model. The geopotential field is averaged over such latitudinal belt in order to derive a one dimensional longitudinal field representative of the atmospheric variability at mid-latitudes (we have verified that the results presented below are quite robust with respect to the selection of the latitudinal band; this is compatible with the fact that they mainly refer to large scale, coherent atmospheric features). Two proxies of dynamical state for large scale features of the mid-latitude troposphere are extracted from such datasets, according to the following procedure:

1. the 500hPa geopotential height field $Z(\lambda, \phi)$ is averaged with respect to latitude ϕ over the latitudinal band bounded between $30°$N and $60°$N;

2. for each day in the DJF period, the 500hPa geopotential height is Fourier decomposed in the longitudinal direction λ;

3. the index is finally computed from the variance associated to the Fourier coefficients Z_k of the zonal wavenumbers, for $k = k_1, k_1 + 1, \ldots, k_n$:

$$Z_{k_1,k_n}(t) = \left(\sum_{k=k_1}^{k_n} 2|Z_k(t)|^2 \right)^{\frac{1}{2}}. \tag{1}$$

The Wave Activity Index (Hansen and Sutera 1986; Benzi et al. 1986), or WAI, is then computed as the root mean square of the zonal wavenumbers 2 to 4 of the winter 500hPa geopotential height variance over the channel $30°$N - $60°$N, that is, formula (1) with $k_1 = 2$ and $k_n = 4$. Furthermore, an index of large scale synoptic disturbances has been computed using $k_1 = 6$ and $k_n = 8$: we refer to this as the Baroclinic Activity Index (BAI). The physical meaning of the WAI and BAI indexes introduced above is further discussed in Sec. 3.

2c. *Statistical inference of extreme values*

The model chosen for the statistical analysis of extremes is the generalised distribution of extreme values (GEV), defined by

$$G(x) = \exp\left\{-\left[1+\xi\left(\frac{x-\mu}{\sigma}\right)\right]^{-1/\xi}\right\}, \tag{2}$$

for x in the set $\{x:\ 1+\xi(x-\mu)/\sigma\ >\ 0\}$ and $G(x) = 0$ otherwise. For $\xi = 0$, the GEV reduces to the Gumbel distribution:

$$G(x) = \exp\left(-\exp\left(-\frac{x-\mu}{\sigma}\right)\right), \tag{3}$$

defined in $x \in \mathbb{R}$. Given a time series, the distributional parameters (μ, σ, ξ) are inferred by maximum likelihood procedures from sequences of block-maxima extracted from the time series. The methodology has been described in detail in Felici et al. (2006a,b), also see Coles (2001) for basic theory and more examples.

A convenient way to summarise the statistical properties of extreme values is the *return level*. Given a number p with $0 < p < 1$, the return level associated with the *return period* $1/p$ is defined as the value z_p that has a probability p to be

exceeded by the block-maxima of the time series. A maximum likelihood estimator for z_p is obtained by plugging the estimates for (μ, σ, ξ) into the formulas for the quantiles of $G(x)$, obtained by inverting (2):

$$\widehat{z}_p = \begin{cases} \widehat{\mu} - \frac{\widehat{\sigma}}{\widehat{\xi}} \left\{ 1 - [-\log(1-p)]^{-\widehat{\xi}} \right\} & \text{for } \widehat{\xi} \neq 0, \\ \widehat{\mu} - \widehat{\sigma} \log[-\log(1-p)] & \text{for } \widehat{\xi} = 0. \end{cases} \tag{4}$$

Confidence intervals for z_p may be obtained from those of (μ, σ, ξ) by the *delta method* (Coles 2001; Felici et al. 2006a).

3. Bulk statistical properties of the model runs

Figure 1 portraits the empirical probability density functions (PDFs) of the WAI and BAI indexes for the control run and the $5CO_2$ case. The PDFs are estimated using the kernel estimation technique of Silverman (1986), where the smoothing parameter h has been chosen as a Gaussian best-fit for each index. We observe that no gross discrepancies are apparent between the two different CO_2 concentration cases; nevertheless, the one-dimensional Kolmogorov-Smirnov test indicates that both pairs of the WAI and of the BAI time series are drawn from different underlying PDFs with a very high degree of confidence. Regarding the first sta-

tistical moments of the time series (see Table 1), we first note that both the mean value and the standard deviation of WAI are much larger than those of BAI, thus confirming that a large portion of the wave activity is concentrated on the spatial scales pertaining to the planetary waves (Dell'Aquila et al. 2005; Lucarini et al. 2006a). The mean values of both WAI and BAI decrease when the CO_2 is increased, even if the 95% confidence bands of the means overlap. Such confidence intervals have been computed using a block-bootstrap method which takes care of the time auto-correlation of the time series. Basically we have that the variance of the mean varies as $s/(L/\tau)$, where s is the sample variance, L is the length of the time series and τ is its decorrelation time. We have that in both cases $\tau \approx 6$ for the BAI and $\tau \approx 12$ for the WAI time series. The standard deviation of WAI and BAI does not change with the CO_2 concentration.

3a. *Interpretation of the results*

The interpretation of the changes of the statistical properties of the BAI and WAI time series due to the alteration in the atmospheric composition requires the analysis of the changes in basic atmospheric fields. When comparing the $5C0_2$ case to the control run, we observe an increase in the global mean surface temperature, a decrease in the surface air meridional temperature gradient in the mid-latitudes

of the northern hemisphere and a widespread increase in the moisture content in the atmosphere. These changes are rather robust features of any climate change simulation entailing increases in CO_2 concentration and the corresponding figures are thus not reported here. We have to emphasise that since we are considering an atmosphere-only model, where the SST and the sea ice-cover fields are kept constant in the two experiments, the observed climate change is greatly reduced with respect to what simulated in a fully coupled atmosphere-ocean models. The decrease of the meridional temperature gradient at surface level is mainly due to the polar amplification effect of the warming caused by the enhanced decrease in the snow cover in the mid-to-high latitudes, particularly over the Siberia, and the consequent decrease of the average albedo in those areas. The $5CO_2$ scenario simulation shows an increase in the surface temperature at mid-to-high latitudes of about 2 degrees. The increase in the moisture content of the atmosphere is related to the enhanced capacity of a warmer atmosphere to retain larger amounts of water vapour. When considering lower pressure levels, the change in the meridional temperature gradient is the opposite, with a strong increase with latitude for the $5CO_2$ case.

Two mechanisms contribute to this effect. First, with varied atmospheric composition, the atmospheric water vapour increase is uneven globally, in such a way

that the moist adiabatic lapse rate decreases in absolute value more in the tropical regions. This tends to offset more and more efficiently going towards lower pressure the decrease in average baroclinicity occurring near the surface. A second possible mechanism is the reduction of the upward propagation of waves into the stratosphere due to the eddy control of the surface meridional gradient.

GCM experiments for climates with reduced equator-to-pole temperature difference (Rind 1998), and for doubled CO_2 (Shindell et al 1998) show such a reduction in planetary wave activity. The reduction of the wave activity should reduce the momentum deposition into the stratosphere, which in turn reduces the overturning circulation of the stratosphere (Haynes 1991). The overturning acts to cool the tropical stratosphere and to warm the polar stratosphere (Eluszkiewicz et al. 1996). The final feature associated with the weakening of the stratospheric circulation is the increase of the meridional temperature gradient at low pressure levels. The bulk of the statistics of both baroclinic and planetary waves seem to support that the depression of the average baroclinicity dominates when the conditions with fivefold increase in CO_2 are considered, and that the reduction of planetary waves activity agrees with the increase of the meridional temperature gradient at low pressure levels.

4. Extreme value analysis

In this section we compare the statistics of extreme values of the $1CO_2$ and $5CO_2$ scenarios, see the next subsection. A discussion on the reliability of our choices concerning the statistical inference is postponed to Sec. 4b.

4a. *Comparison of the scenarios*

The statistics of extreme values are analysed in two steps: firstly, the parameters μ, σ and ξ of the GEV distribution (2) are inferred from sequences of maxima and of minima for each of the six time series of WAI and BAI; secondly, return levels are computed for several return periods by using (4). For the estimation of (μ, σ, ξ), each time series is subdivided into B data blocks, each containing D daily values, where $B = L/D$ and L is the total length (number of daily observations) of the time series. Maximum values of the indexes over each data block are computed, yielding sequences of extreme values from which (μ, σ, ξ) are inferred. The same procedure is applied to sequences of block minima of the time series. For D we have selected two values: $D = 100$ and $D = 200$. The corresponding point estimates and uncertainties of the GEV parameters are reported in Tabs. 2 and 3 for the block maxima and in Tabs. 4, 5 for the block minima.

Plots of the return levels z_p as functions of the return period $1/p$ are given in Fig. 2 (for $D = 100$) and in Fig. 3 (for $D = 200$), both for the maxima and for the minima of the time series. For the minima we obtain negative values since in this case the inferences are performed by first multiplying the time series for -1 and then extracting the maxima. In each plot results for both the time series $1CO_2$ and $5CO_2$ are given together, to allow comparison. It turns out that the differences, at extreme levels, between the $1CO_2$ scenario and the $5CO_2$ scenarios are not particularly significant, from the statistical point of view: the best estimates of the return levels for $5CO_2$ fall in most cases within the confidence intervals of the $1CO_2$ simulation and vice versa. Where the estimated uncertainty is smaller, one has that the point estimates agree with higher precision. The only exception is provided by the minima of the WAI index, for which the confidence intervals of the run with $1CO_2$ do not overlap with those of the $5CO_2$ case, at least for sufficiently large return periods.

The large sampling uncertainty of the time series suggests that it may be dangerous to draw physical conclusions from the mere comparison of the point estimates of the GEV parameters: confidence intervals should always be taken into account in the analysis. We also emphasise that it may be misleading to identify changes in the point estimates of the location parameter μ with changes in the

"average extremes": an example of this is provided by the maxima of the WAI index, for which, when passing from $1CO_2$ to $5CO_2$, one observes an increase of μ but a decrease in the return levels (at least for sufficiently large return periods). Both differences are, however, not very significant (particularly so for the point estimate of μ), given the overlapping of the confidence intervals.

We also remark that the inferred value of the parameter ξ is negative, corresponding to a Weibull distribution (Coles 2001). The support of Weibull probability density functions is bounded from above: there exists a value $z_\infty = \mu - \sigma/\xi$ which may be considered as a return level with unbounded return period, since values larger than z_∞ form a set having zero probability (the Weibull probability density function is identically zero for those values). The fact that ξ is negative with overwhelming reliability suggests the existence of upper and lower bounds for the considered indexes. Since we are dealing with global variables, we may attribute this property to fact that the system we analyse has a finite energy input; see the related discussion in the context of a simpler model analysed by Felici et al. (2006a).

4b. *Assessment and sensitivity analysis*

The data block size D has been determined by trying several values of n and assessing goodness-of-fit by standard diagnostics. Since the GEV is a limit distribution, obtained in the limit of L and D going to infinity, in order to catch genuinely extreme events it is not sufficient to take a block length that is slightly larger than the decorrelation time scale τ. This implies that 50 days is likely to be the minimum acceptable block length. We also emphasise that there is no need to detrend the data in the present analysis, since the runs with the ECHAM4.6 model are performed under perpetual January conditions. Although the latter is an oversimplification of the model, as far as inference of extreme values is concerned, statistical stationarity is an important advantage offered by the considered ECHAM4.6 simulations with respect to other models or observed data. See the discussion in Felici et al. (2006b).

The influence of the choice of block length D is illustrated in Fig. 4, where we display the inferred values of the GEV parameter ξ (and the related uncertainties) against the value of D used for the inference. The asymptotic nature of the GEV distribution reflects to the fact that the inferences become approximately constant as D increases. Of course, uncertainties increase with D, since one is using less values for the inference. Accordingly, the values of D of the previous section (that

is $D = 100$ and 200) are selected in such a way that the inferences are reasonably stable and that the associated uncertainties are not too large. There is a good deal of subjectivity in this choice: as usual in GEV-based analysis (Coles 2001; Felici et al. 2006a,b), one has to adopt a reasonable compromise between long and short data blocks. Using long data blocks is more likely to yield sequences of "genuine" extremes, but fewer values are selected, which may result in unacceptably large uncertainties. Taking too short block sizes, however, might induce a bias towards the bulk of the statistics (or even cause problems due to a non-negligible amount of autocorrelation in the data). This problem is particularly serious when dealing with real observations, since we cannot extend the length of the record to satisfy the requirements on data abundance.

For all time series of WAI and BAI, the choice of $D = 100$ is reasonable: it is large enough to ensure decorrelation of the extreme values and, moreover, the point estimates of the GEV parameters remain almost constant for $D \geq 100$. Moreover the maximum likelihood estimate of ξ is is always negative, except in cases where sampling uncertainty is large, see Fig. 4. The diagnostic plots in Fig. 5 confirm that both choices $D = 100$ and $D = 200$ yield inferences of reasonably good quality: for example, the displacements of points from the diagonals are relatively small in the probability and quantile plots. More graphical

diagnostics (not shown), analogous to those in Fig. 4 and Fig. 5, suggest that the same conclusions also hold for the minima.

The similarities of the statistics of extreme values between the two scenarios are further highlighted in Fig. 6: the GEV probability densities nearly overlap. A word of caution should be spent here because a small variation in the probability density corresponds to a huge difference in total wave energy for the WAI index, whereas this difference is much smaller for BAI. Although sharper discrepancies appear for larger D, the corresponding return values (not shown) are in fact rather similar for the two CO_2 scenarios. This suggests that the differences in the GEV densities are not particularly significant: they seem to be due to sampling uncertainty, related to excessive shortness of the record, rather than to a relevant variation of the underlying physical processes. Our confidence in this statement is based on the numerous diagnostic plots that we have examined (not shown), that include many more plots similar to those in Figs. 3 up to 6, but also non-parametric densities, estimated from the sequences of maxima and minima and also the visual inspection of the maps reported in Sec. 5.

5. Mapping the extremes

In this section we examine the average maps corresponding to the sequences of extreme values (maxima or minima) extracted from the time series of the WAI and BAI indexes. For each index, maxima and minima are computed over blocks of length $D = 100$ days (see Sec. 4a). From these extreme value samples, we selected the 500hPa maps corresponding to the date of the extremes. Collecting these *maps of extremes* in four ensembles, we computed the mean and the standard deviation for each ensemble.

Fig. 7 shows the ensemble eddy mean and the ensemble standard deviation (denoted by std for shortness) for both the $5CO_2$ and $1CO_2$cases (left and right columns, respectively) of the maxima. Visual inspection suggests an amplification of wave number 2 and 3 for the eddy fields. The WAI case (top row) shows enhanced eddy field, as expected by the choice of the index, with increasing of the positive centre over the Rockies and deepening of the negative centre over the Labrador with respect to the mean eddy field, where the latter mean (not shown) is taken over the whole time series. This wavy pattern corresponds to a ridge over the Rockies and diffluent flow over Europe. For the $5CO_2$ case, we observe an increase of the geopotential height over the Siberian plateau and a moderate westward shift of the wave pattern respect to the $1CO_2$ case. The std patterns

display two main peaks over the north-central Atlantic and over the north-western Pacific. Those peaks correspond to the ending part of the two oceanic storm-track regions, in correspondence with the jet exit for both the oceanic sectors. The $5CO_2$ run shows higher values over the Euro-Atlantic sector, while the $1CO_2$ over the Pacific.

The BAI case (bottom panel) shows an eddy pattern similar to the mean eddy pattern (figure not shown). Moreover the differences between $5CO_2$ and $1CO_2$ runs bear some resemblance to the differences between the corresponding total means. In particular, the $1CO_2$ run is characterised by an eastward shift over the Rockies and a northward shift of the Euro-Atlantic positive anomaly. The two std maps show larger variance in correspondence with the bandpass-high frequency filtered 500hPa height variance, which characterises the storm-track areas. A noteworthy fact is that the extremes of a planetary index, as is our BAI, contain information on the regional storm-tracks.

Fig. 8 shows the same plots as in Fig. 7, but for the minima of the indexes. The WAI case (top panel) displays a strong zonal flow, which is characterised by the wave number 1 in the eddy field, as expected by the choice of the index. The difference between the two total fields (figure not shown) suggests a zonal increase of the 500hPa geopotential height around the globe for the $5CO_2$ case

The WAI minima ensembles show std centres in the exit region of the Pacific jet and over the northern Atlantic. As previously noted, the BAI case (bottom panels) shows an eddy pattern similar to the mean eddy pattern (figure not shown), while the two std maps show larger variance in correspondence with the Pacific and Atlantic jet exit regions.

6. Summary and conclusions

We have analysed the impact of a five-fold increase in atmospheric CO_2 on the statistics of two wave indexes in the ECHAM4.6 General Circulation Model. The indexes we have examined can be considered as proxies of wave activity at different spatial and temporal scales. The investigation shows that, although certain differences are observed between the simulation at $1CO_2$ and that with $5CO_2$, these differences are not dramatic. As far as the whole statistics of the time series is concerned, we observe that the average low frequency-low wavenumber activity, as well as the high frequency baroclinic activity, clearly show a slight shift to lower value when going from 1 to $5CO_2$. This can be interpreted as the effect of the decrease of the average baroclinicity of the mid-latitudes, which is only partially offset by the potentially storm-enhancing effect due to the increase of the

moisture content of the atmosphere. We note that, in a fully coupled simulation of climate, it is likely that both effects of depression of the average baroclinicity of the system and increase in the moisture content of the atmosphere for increased CO_2 concentration are greatly enhanced. Therefore, it is unclear whether the overall impact would be the same as in the present simulations.

The statistical behaviour of extreme values of the various time series is studied by the block-maximum method, by inferring Generalised Extreme Value models. The statistical significance of these results has been thoroughly assessed by standard diagnostic tools. The results indicate that the often invoked approach of relating changes of the extremes to changes in the mean and standard deviation of the bulk statistics is not very reliable: in the present case, for the time series smaller means and same variances are obtained when passing from 1 to $5CO_2$ (compare Table 1), but there is little or no change at extreme levels (compare Fig. 2). Moreover, even for the present, idealised simulations, large uncertainties (confidence intervals) are systematically obtained in the estimates of the GEV. This suggests that very long time series are required for accurate estimations and this problem is likely to be harder when dealing observed data or with non-stationary simulations (*e.g.* including the seasonal cycle). Also, the results indicate that the identification of changes in the point estimates of the GEV parameters μ and σ with changes

in the overall statistical properties of the extremes is questionable: for instance, a larger point estimate of μ does not necessarily imply larger return levels. In this sense, the value of the parameter ξ, which is usually the most delicate to estimate, plays a crucial role. This is particularly relevant for the extrapolation of the inferences at very high levels. The analysis of extreme values is complemented by an examination of composite maps of the extremes of the maxima. The main feature we observe is that the increase of the CO_2 concentration tends to increase the relative weight of the wave activity of the Atlantic sector.

In this study, we considered global measure of physical waves experienced by the atmospheric system. An important step forward will be to consider local measure of climatic parameters, such as precipitation or surface temperature, for generalising the results of the present work. However, we emphasise that the examination of variables of local nature is likely to be more problematic: compare *e.g.* Vannitsem (2007), where it is suggested that prohibitively long time series are necessary to reach satisfactory convergence of the statistical estimators. This conclusion further highlights the need of understanding the physical processes which should be involved in the change of meteo-climatic extremes, in parallel with the study of the statistical properties of models of ever-increasing complexity.

References

Coles, S., 2001: *An Introduction to Statistical Modelling of Extremes Values*. Springer-Verlag, 208 pp.

Benzi, R. and A. Speranza, 1989: Statistical properties of low frequency variability in the Northern Hemisphere. *J. Climate*, **2**, 367–379.

Benzi R., P. Malguzzi., A. Speranza and A. Sutera, 1986: The statistical properties of general atmospheric circulation: observational evidence and a minimal theory of bimodality. *Quart. J. Roy. Met. Soc.*, **112**, 661–674.

Blackmon, M.L., 1976: A climatological spectral study of the 500 mb geopotential height of the Northern Hemisphere. *J. Atmos. Sci.*, **33**, 1607–1623.

Buzzi, A., A. Trevisan, and A. Speranza, 1984: Instabilities of a baroclinic flow related to topographic forcing. *J. Atmos. Sci.*, **41**, 637–650.

Charney, J.G., and J.G. DeVore, 1979: Multiple Flow Equilibria in the Atmosphere and Blocking. *J. Atmos. Sci.*, **36**, 1205–1216.

Charney, J.G., and P.G. Drazin, 1961: Propagation of planetary-scale disturbances from the lower into the upper atmosphere. *J. Geophys. Res.*, **66**, 83–109.

Charney, J.G., and A. Eliassen, 1949: A numerical method for predicting the perturbations of the midlatitude westerlies. *Tellus*, **1**, 38–54.

Charney, J.G., and D.M. Straus, 1980: Form-Drag Instability, Multiple Equilibria and Propagating Planetary Waves in Baroclinic, Orographically Forced, Planetary Wave Systems. *J. Atmos. Sci.*, **37**, 1157–1176.

Dell'Aquila, A., V. Lucarini, P.M. Ruti, and S. Calmanti, 2005: Hayashi Spectra of the Northern Hemisphere Mid-latitude Atmospheric Variability in the NCEP-NCAR and ECMWF Reanalyses. *Climate Dynamics*, DOI: 10.1007/s00382-005-0048-x.

Dell'Aquila, A., P.M. Ruti, A. Sutera, 2006: Baroclinic adjustement of the tropopause in the NCEP-NCAR reanalysis. *Clim. Dyn.*, DOI 10.1007/s00382-006-0199-4.

Eluszkiewicz, J., D. Crisp, R. Zurek, L. Elson, E. Fishbein, L. Froidevaux, J. Waters, R.G. Grainger, A. Lambert, R. Harwood, and G. Peckham, 1996: Residual circulation in the stratosphere and lower mesosphere as diagnosed from Microwave Limb Sounder data. *J. Atmos. Sci.*, **53**, 217–240.

Fasano, G., and A. Franceschini, 1987: A multidimensional version of the Kolmogorov-Smirnov test. *Mon. Not. R. Astr. Soc.*, **225**, 155–170.

Felici, M., V. Lucarini, A. Speranza, and R. Vitolo, 2007: Extreme Value Statistics of the Total Energy in an Intermediate Complexity Model of the Mid-latitude Atmospheric Jet. Part I: Stationary case. To appear in *J. Atmos. Sci.*.

Felici, M., V. Lucarini, A. Speranza, and R. Vitolo, 2007: Extreme Value Statistics of the Total Energy in an Intermediate Complexity Model of the Mid-latitude Atmospheric Jet. Part II: Trend Detection and Assessment. To appear in *J. Atmos. Sci.*.

Fouquart, Y. and B. Bonnel, 1980: Computations of solar heating of the Earth's atmosphere: a new parametrization. *Contrib. Phys. Atm.*, **53**, 35–62.

Hansen, A.R., and A. Sutera, 1986: On the probability density distribution of planetary-scale atmospheric wave amplitude. *J. Atmos. Sci.*, **43**, 3250–3265.

Hansen, A.R., and A. Sutera, 1995: The probability density distribution of Planetary-Scale Atmospheric Wave amplitude Revisited. *J. Atmos. Sci.*, **52**, 2463–2472.

Hayashi, Y., 1971: A generalized method for resolving disturbances into progressive and retrogressive waves by space Fourier and time cross-spectral analysis. *J. Meteorol. Soc. Jpn.*, **49**, 125–128.

Hayashi, Y., 1979: A generalized method for resolving transient disturbances into standing and travelling waves by space-time spectral analysis. *J. Atmos. Sci.*, **36**, 1017–1029.

Haynes, P.H., C.J. Marks, M.E. McIntyre, T.G. Shepherd, and K.P. Shine., 1991: On the downward control of extratropical diabatic circulations by eddy induced mean zonal forces. *J. Atmos. Sci.*, **48**, 651–679.

Holton, J. R., 1992: *An Introduction to Dynamic Meteorology*. 2nd ed., Academic Press, 391 pp.

Lucarini, V., S. Calmanti, A. dell'Aquila, P. M. Ruti, and A. Speranza, 2006: Intercomparison of the northern hemisphere winter mid-latitude atmospheric variability of the IPCC models. *Clim. Dyn.*, DOI: 10.1007/s00382-006-0213-x.

Lucarini, V., A. Speranza, and R. Vitolo, 2006: Physical and Mathematical Properties of a Quasi-Geostrophic Model of Intermediate Complexity of the Mid-Latitudes Atmospheric Circulation. *Preprint* `ArXiv, DOI:physics/0511208`, submitted.

V. Lucarini, A. Speranza, R. Vitolo: Self-Scaling of the Statistical Properties of a Minimal Model of the Atmospheric Circulation, to appear in *20 Years of Non-*

linear Dynamics in Geosciences, Eds. J. Elsner, A. Tsonis, Springer (New York, USA) (2007).

Malguzzi, P., and A. Speranza, 1981: Local Multiple Equilibria and Regional Atmospheric Blocking. *J. Atmos. Sci.*, **38**, 1939–1948.

Malguzzi, P., A. Speranza, A. Sutera, R. Caballero, 1997: Nonlinear amplification of stationary Rossby waves near resonance, Part II. *J. Atmos. Sci.*, **54**, 2441–2451.

Miller, M.J., T.N. Palmer, and R. Swinbank, (1989): Parameterization and influence of sub-grid scale orography in general circulation and numerical weather prediction models. *Meteorol. Atmos. Phys.*, **40**, 84–109.

Morcrette, J.J., 1991: Radiation and cloud radiative properties in the European Center for Medium Range Forecasts forecasting system. *J. Geophys. Res.*, **96**, 9121–9132.

Morcrette, J.J., and C. Jakob, 2000: The Response of the ECMWF Model to Changes in the Cloud Overlap Assumption. *Mon. Wea. Rev*., **128**, 1707–1732.

Guilyardi, E., P. Delecluse, S. Gualdi, and A. Navarra, 2002: Mechanisms for ENSO Phase Change in a Coupled GCM. *J. Climate*, **16**, 1141–1158.

Nordeng, T.E., 1994: Extended versions of the convective parameterization scheme at ECMWF and their impact on the mean and transient activity of the model in the tropics. ECMWF, Technical Memo n. 206, Reading, England, 41 pp.

Rind, D., 1998: Latitudinal temperature gradients and climate change. *J. Geophys. Res.*, **103**, 5943–5971.

Roeckner, E., 1995: Parameterization of cloud radiative properties in the ECHAM4 model. In Proceedings of the WCRP Workshop: cloud microphysics parameterizations in global circulation models, WCRP Report n. 93, WMO/TD-no 713, 105-116.

Roeckner, E., and K. Arpe, 1995: AMIP experiments with the new Max Planck Institute for Meteorology Model ECHAM4. In: Proceedings of the "AMIP Scientific Conference", May 15-19, 1995, Monterey, USA, WCRP-Report No. 92, 307-312, WMP/TD-No. 732.

Roeckner E., R. Brokopf, M. Esch, M. Giorgetta, S. Hagemann, L. Kornblueh, E. Manzini, U. Schlese, U. Schulzweida., 2004: The atmospheric general circulation model ECHAM 5. PART II: Sensitivity of Simulated Climate to Horizontal and Vertical Resolution, MPI-Report 354, 56 pp, 2004.

Ruti, P.M., V. Lucarini, A. dell'Aquila, S. Calmanti, and A. Speranza, 2006: Does the subtropical jet catalyze the midlatitude atmospheric regimes? *Geophys. Res. Lett.*, **33**, L06814, doi:10.1029/2005GL024620.

Simmons, A. J., D. M. Burridge, M. Jarraud, C. Girard and W. Wergen, 1989: The ECMWF medium-range prediction models: Development of the numerical formulations and the impact of increased resolution. *Meteorol. Atmos. Phys.*, **40**, 28–60.

Shindell, D. T., D. Rind, and P. Lonergan, 1998: Increase polar stratospheric ozone losses and delayed eventual recovery owing to increasing green-house-gas concentrations. *Nature*, **392**, 589–592.

Speranza, A., 1983: Deterministic and statistical properties of the Westerlies. *Paleogeoph.*, **121**, 512–562.

Sutera, A., 1986: Probability density distribution of large scale atmospheric flow. *Adv. Geophys.*, **29**, 319-338.

Silverman, B.W., 1986: *Density Estimation for Statistics and Data Analysis*. Chapman & Hall.

Tiedke, M., 1989: A comprehensive mass flux scheme for cumulus parameterization in large-scale models. *Mon. Wea. Rev.*, **117**, 1779–1800.

Vannitsem, S., 2006: Statistical Properties of the Temperature Maxima in an intermediate order QG model. *Tellus A*, **59**, 80-95.

Wallace, J.M., G. Lim, and M.L. Blackmon, 1988: Relationship between Cyclone Tracks, Anticyclone Tracks and Baroclinic Waveguides. *J. Atmos. Sci.*, **45**, 439–462.

Williamson, D. L., and P. J. Rasch, 1994: Water vapour transport in the NCAR CCM2. *Tellus*, **46A**, 34–51.

Zhang, X., F. W. Zwiers, and G. Li, 2003: Monte Carlo Experiment on the Detection of Trends in Extreme Values. *J. Climate*, **17**, 1945–1952.

Zwiers, F. W., and V. V. Kharin, 1998: Changes in the Extremes of the Climate Simulated by CCC GCM2 under CO_2 Doubling. *J. Climate*, **11**, 2200–2222.

Kharin, V. V., and F. W. Zwiers, 2000: Changes in the Extremes in an Ensemble of Transient Climate Simulations with a Coupled Atmosphere-Ocean GCM. *J. Climate*, **13**, 3760–3788.

List of Figures

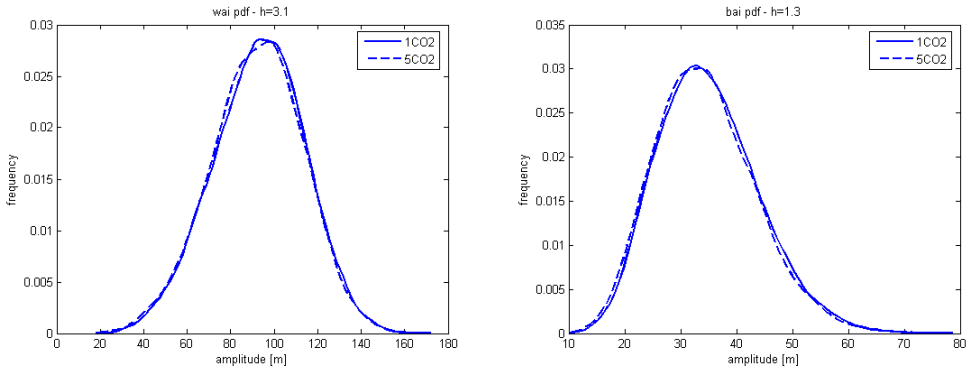

Figure 1: Left: One-dimensional probability distribution function of the planetary wave index WAI for the runs with $1CO_2$ (continuous line) and $5CO_2$ (dashed line). Units: WAI [m]. Right: same as left panel for the BAI index.

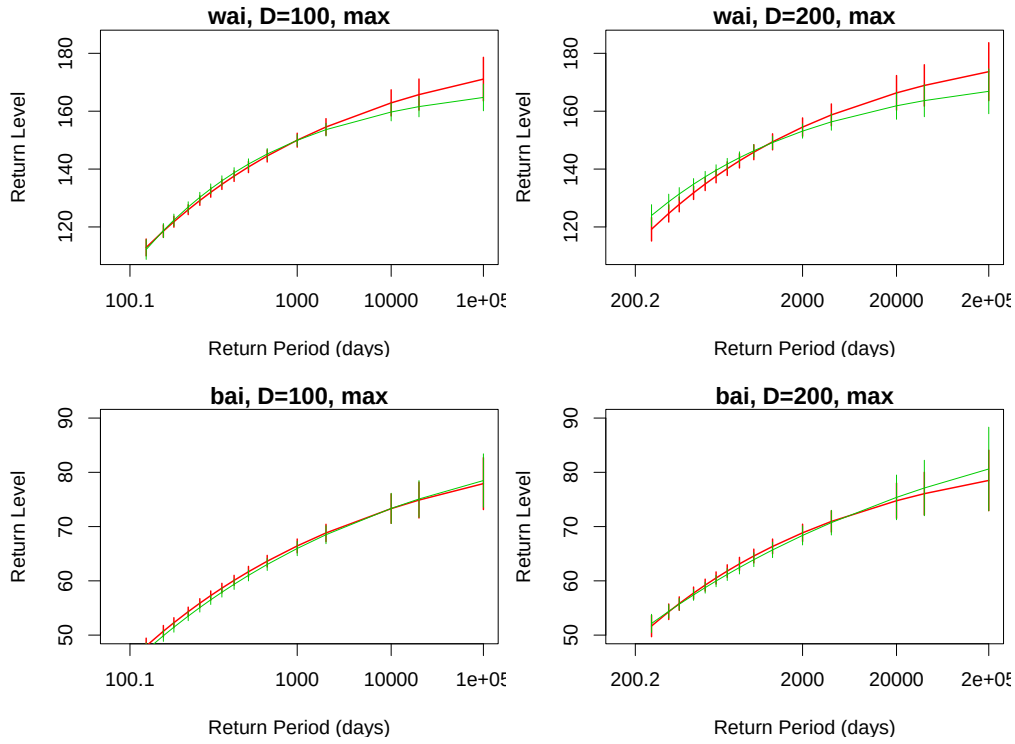

Figure 2: Return level plots for maxima of the the WAI (top row) and BAI (bottom row) time series, using blocks of length $D = 100$ days (left column) and $D = 200$ (right column), for the simulations $1CO_2$ and $5CO_2$, in red and green, respectively.

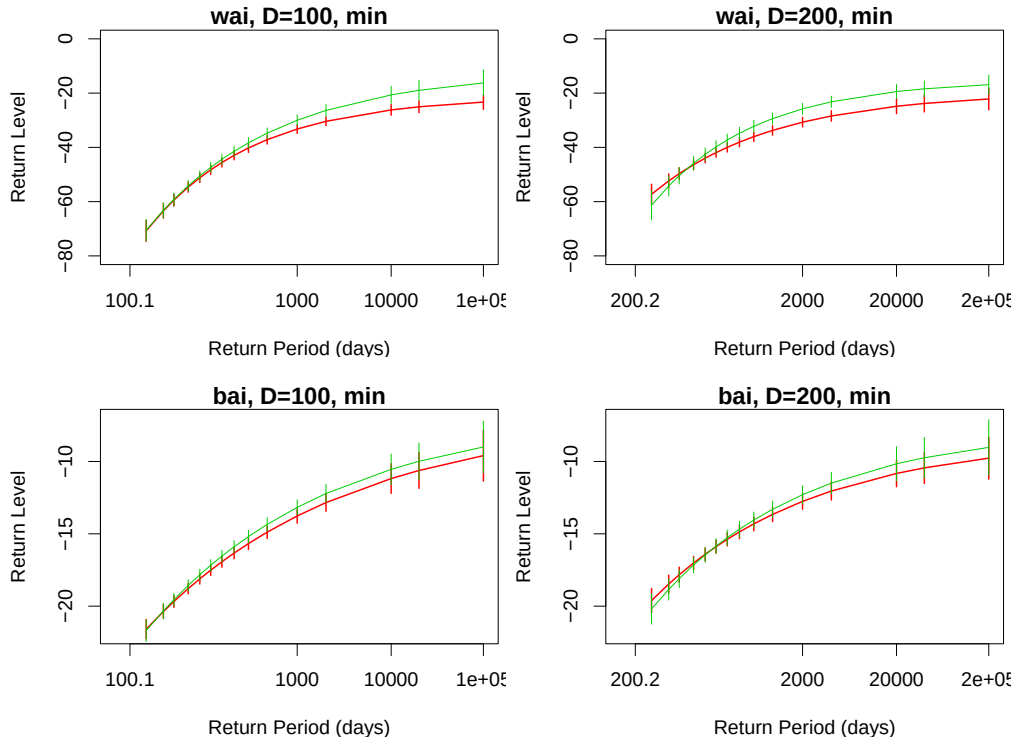

Figure 3: Same as Fig. 2 for minima of the time series.

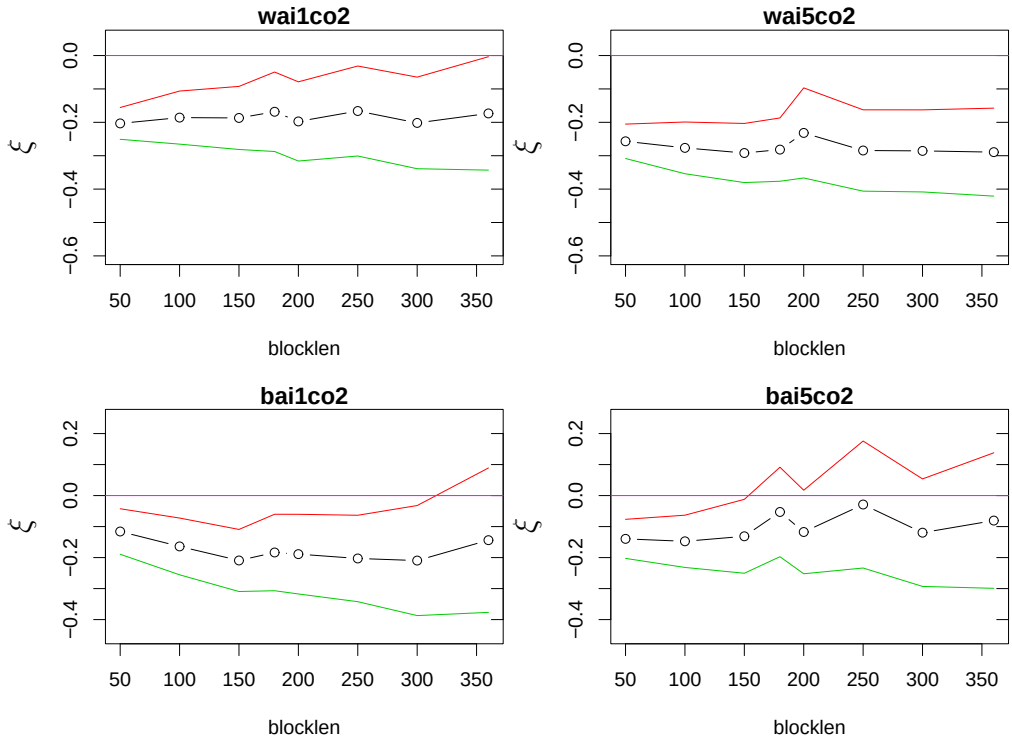

Figure 4: Top row: the inferred value of the shape parameter ξ as a function of the block length D over which maxima are computed, for time series of WAI index for the simulations $1CO_2$ (left panel) and $5CO_2$ (right panel), respectively. 95% confidence intervals (average plus and minus two standard deviations) are added. Second row: same as in the first row for the BAI index.

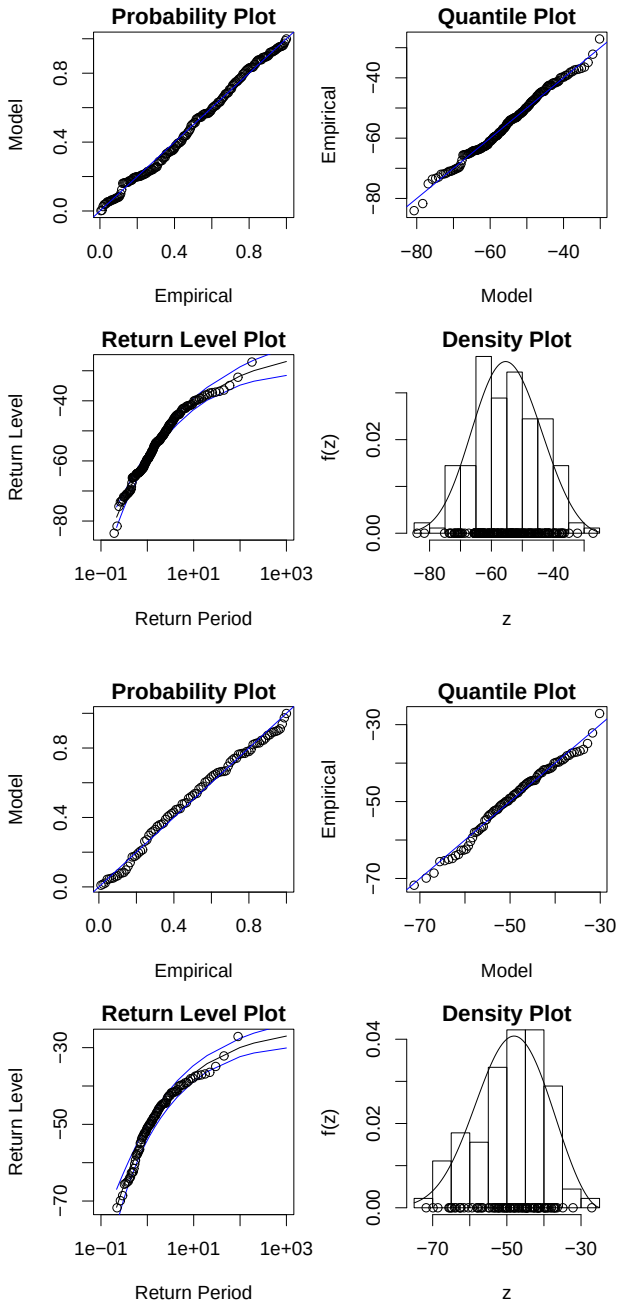

Figure 5: Diagnostic Plots for the sequences of minima of the BAI index for the $5CO_2$ simulation, with $D = 100$ (top) and 200 (bottom).

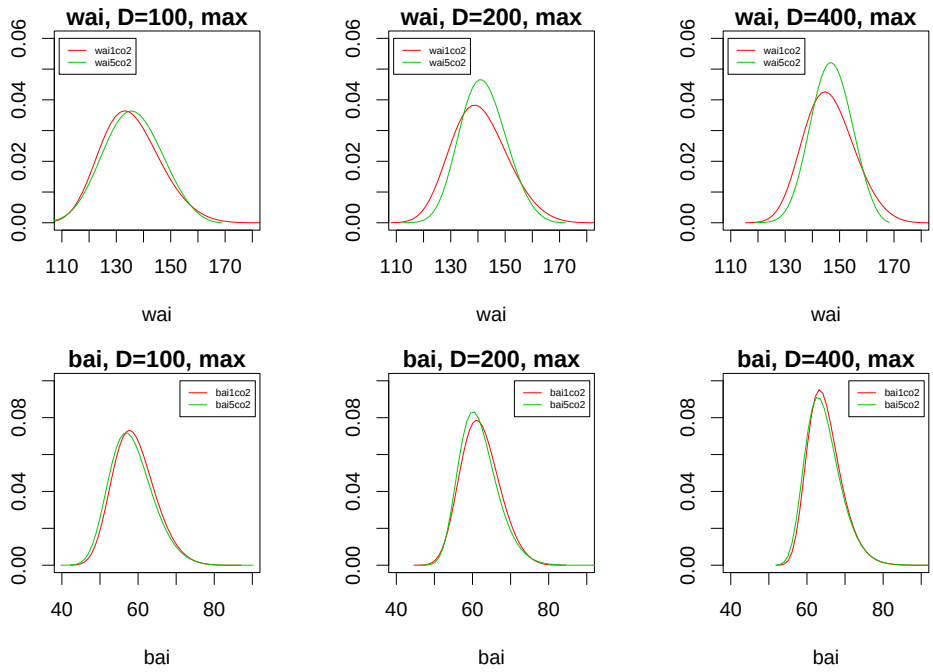

Figure 6: GEV probability density functions inferred from sequences of maxima computed over data blocks of length 100, 200, and 400 (left, middle and right column, respectively), for the WAI and BAI indexes (top and bottom row, respectively), for the simulations $1CO_2$ and $5CO_2$ (red and green, respectively).

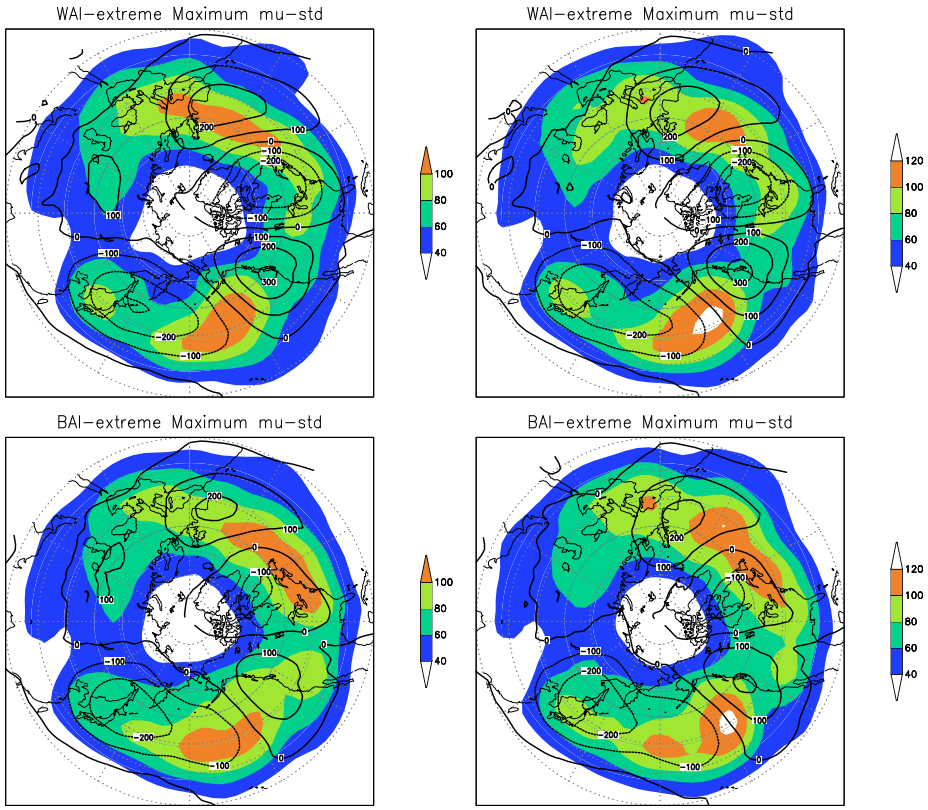

Figure 7: The eddy ensemble mean (contour) and the standard deviation (shaded) of the 100-day maxima of the WAI (top row) and BAI (bottom row) indexes, for the simulations with $5CO_2$ (left panel) and the $1CO_2$ (right panel).

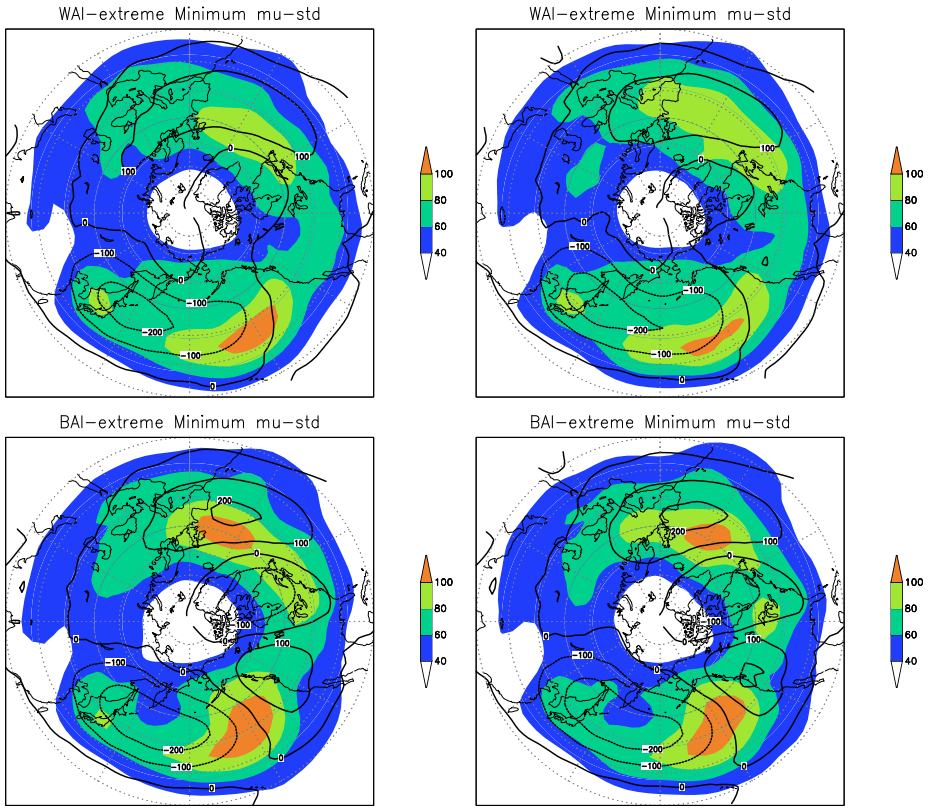

Figure 8: Same as Fig. 7 for the minima of the indexes.

Table 1: 95% confidence band of the mean and standard deviation (both expressed in m) of the WAI and BAI indexes for each of the two GCM runs.

	95% mean confidence band	standard deviation
WAI1CO_2	93.0 ± 1.9	21.0
WAI5CO_2	92.1 ± 1.8	21.1
BAI1CO_2	35.0 ± 0.3	9.0
BAI5CO_2	34.5 ± 0.3	9.0

Table 2: Maximum likelihood estimates of the GEV parameters, inferred from sequences of block-maxima of the WAI and BAI index, with block length $D = 100$, for the two considered simulations: $1CO_2$ and $5CO_2$. Uncertainties are 95% confidence bands, evaluated by the observed information matrix. μ, σ and their statistical uncertainties are expressed in units of m.

	ξ	σ	μ	D	L
WAI1CO2	-0.19 ± 0.04	10.28 ± 0.58	131.08 ± 0.84	100	18000
WAI5CO2	-0.28 ± 0.04	10.55 ± 0.6	132.26 ± 0.85	100	18000
BAI1CO2	-0.16 ± 0.05	5.1 ± 0.29	56.84 ± 0.42	100	18000
BAI5CO2	-0.15 ± 0.04	5.18 ± 0.29	56.05 ± 0.42	100	18000

Table 3: Same as Table 2, with $D = 200$.

	ξ	σ	μ	D	L
WAI1CO2	-0.20 ± 0.06	9.81 ± 0.79	136.68 ± 1.14	200	18000
WAI5CO2	-0.23 ± 0.07	8.13 ± 0.68	138.87 ± 0.95	200	18000
BAI1CO2	-0.19 ± 0.07	4.77 ± 0.38	60.11 ± 0.55	200	18000
BAI5CO2	-0.12 ± 0.07	4.45 ± 0.37	59.58 ± 0.52	200	18000

Table 4: Same as Table 2, for the block-minima of the WAI and BAI indexes.

	ξ	σ	μ	D	L
WAI1CO2	-0.37 ± 0.04	10.48 ± 0.60	-49.18 ± 0.84	100	18000
WAI5CO2	-0.31 ± 0.05	11.35 ± 0.66	-48.34 ± 0.93	100	18000
BAI1CO2	-0.20 ± 0.05	2.18 ± 0.13	-17.70 ± 0.18	100	18000
BAI5CO2	-0.22 ± 0.05	2.37 ± 0.14	-17.38 ± 0.20	100	18000

Table 5: Same as Table 4, with $D = 200$.

	ξ	σ	μ	D	L
WAI1CO2	-0.33 ± 0.06	7.43 ± 0.60	-42.56 ± 0.86	200	18000
WAI5CO2	-0.39 ± 0.06	9.92 ± 0.81	-40.67 ± 1.13	200	18000
BAI1CO2	-0.25 ± 0.06	1.91 ± 0.15	-16.05 ± 0.22	200	18000
BAI5CO2	-0.26 ± 0.07	2.21 ± 0.18	-16.04 ± 0.26	200	18000